Supporting Information

One-pot Synthesis of Zeolitic Imidazolate Framework 67-Derived Hollow Co_3S_4@MoS_2 Heterostructures as Efficient Bifunctional Catalysts

Yanna Guo,[a,b] Jing Tang,[a]* Huayu Qian,[c] Zhongli Wang,[a] and Yusuke Yamauchi[a,b,d]*

[a] International Center for Materials Nanoarchitectonics (MANA), National Institute for Materials Science (NIMS), 1-1 Namiki, Tsukuba, Ibaraki 305-0044, Japan; E-mail: TANG.Jing@nims.go.jp

[b] Faculty of Science and Engineering, Waseda University, 3-4-1 Okubo, Shinjuku, Tokyo 169-8555, Japan

[c] Key Laboratory for Soft Chemistry and Functional Materials of Ministry Education, Nanjing University of Science and Technology, Nanjing 210094, P. R. China

[d] Australian Institute for Innovative Materials (AIIM), University of Wollongong, North Wollongong, NSW 2500, Australia; E-mail: yusuke@uow.edu.au

Figure S1

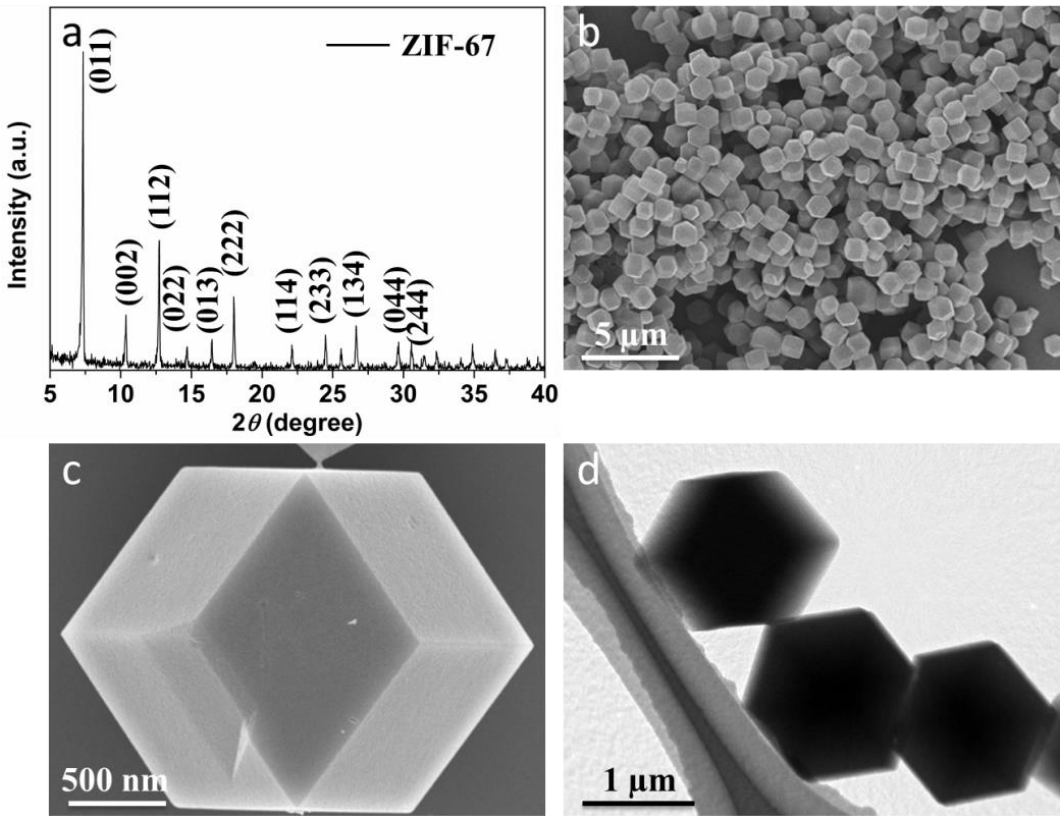

Figure S1. (a) XRD patterns, (b, c) SEM images, and (d) TEM image of ZIF-67 precursors.

Figure S2

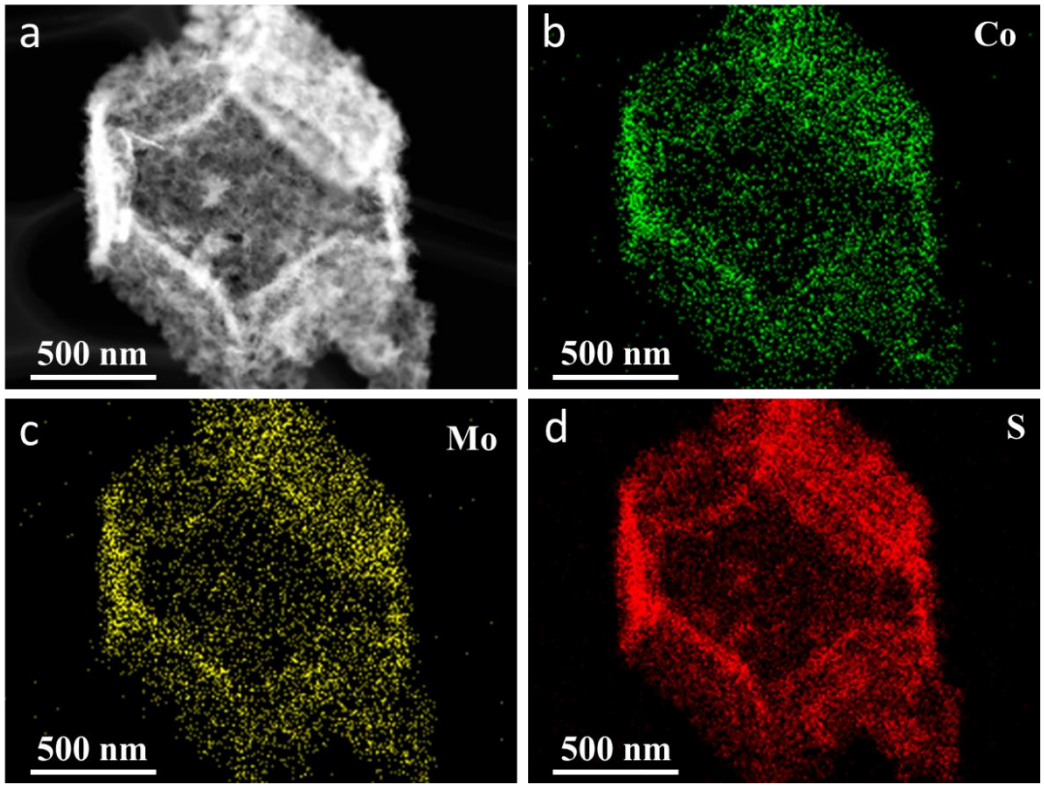

Figure S2. (a) STEM, and (b–d) TEM-EDXS elemental mapping images of hollow Co_3S_4@MoS_2 heterostructures.

Figure S3

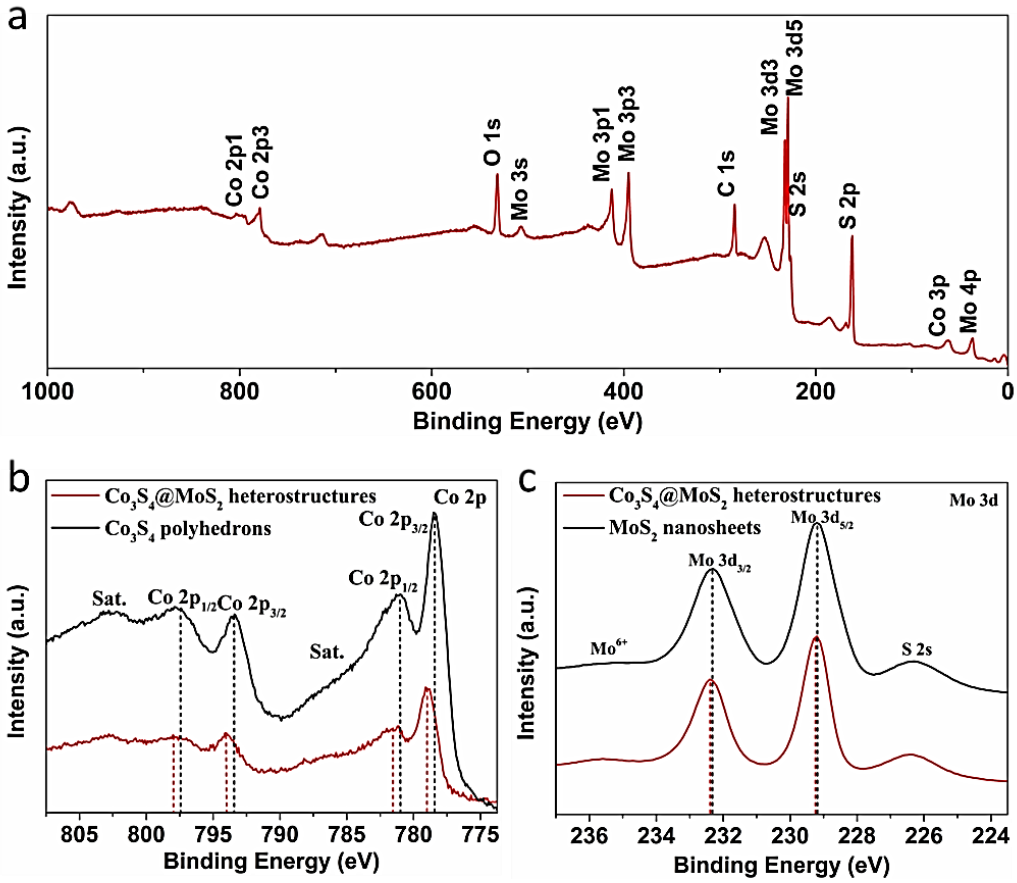

Figure S3. (a) XPS spectrum of Co_3S_4@MoS_2 heterostructures. High-resolution XPS spectrum of (b) Co 2p, and (c) Mo 3d.

Figure S4

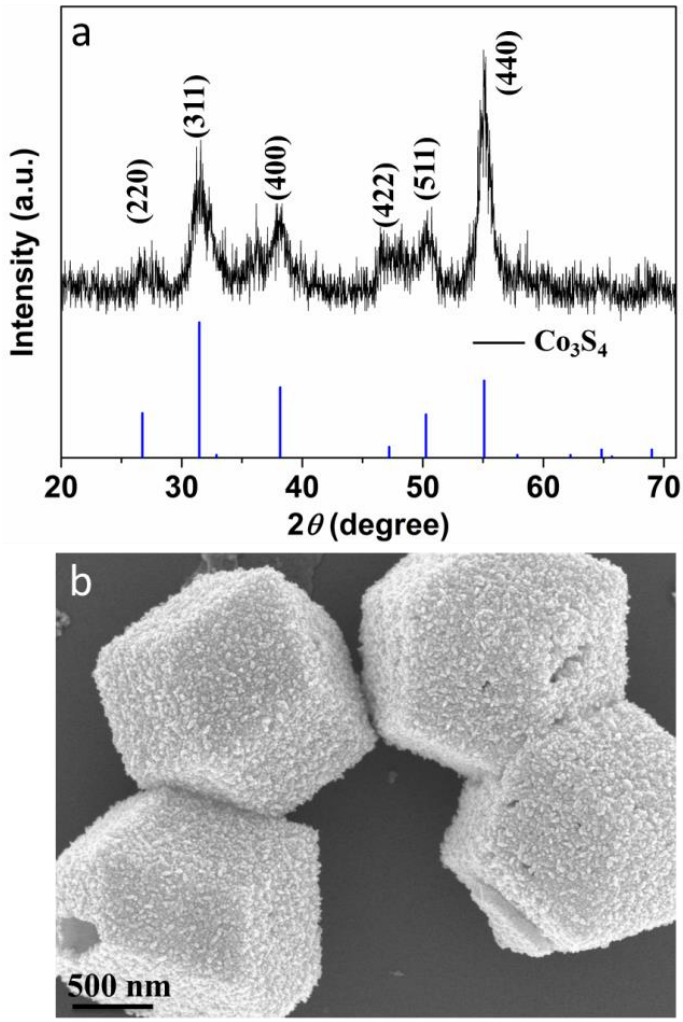

Figure S4. (a) XRD pattern, and (b) SEM image of the intermediate product obtained after hydrothermal reaction at 120 °C for 4 h.

Figure S5

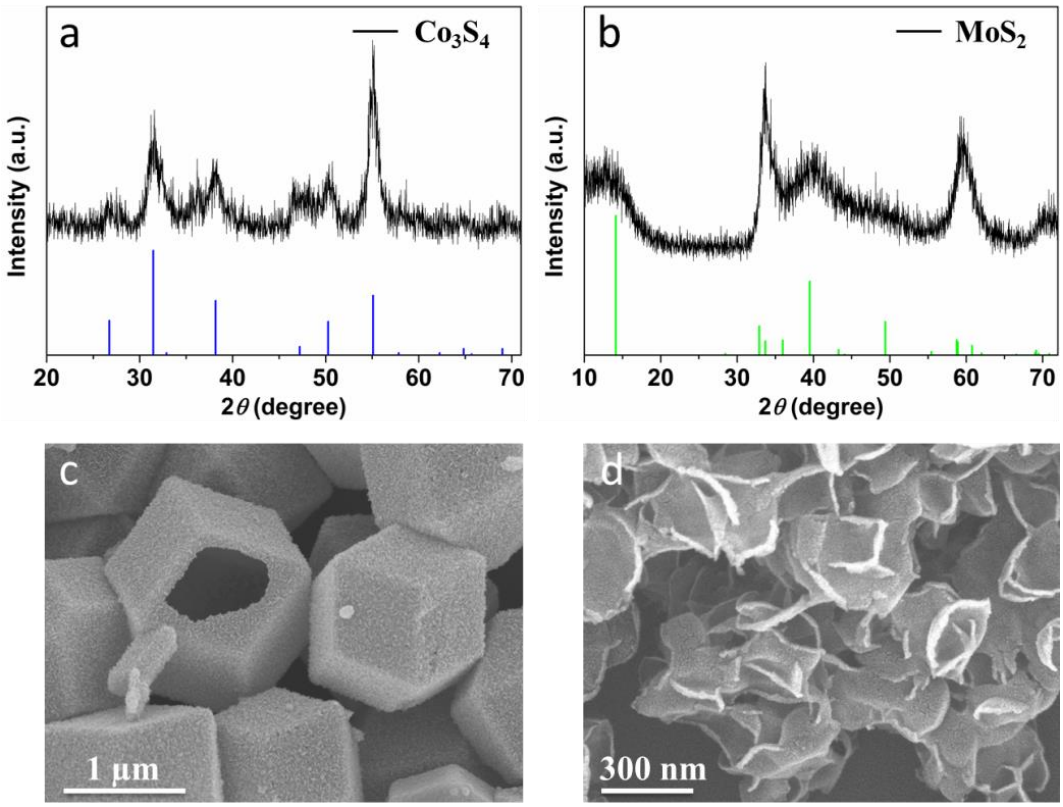

Figure S5. (a,b) XRD patterns, and (c,d) SEM images of individual hollow Co_3S_4 polyhedrons (a,c) and MoS_2 nanosheets (b,d).

Figure S6

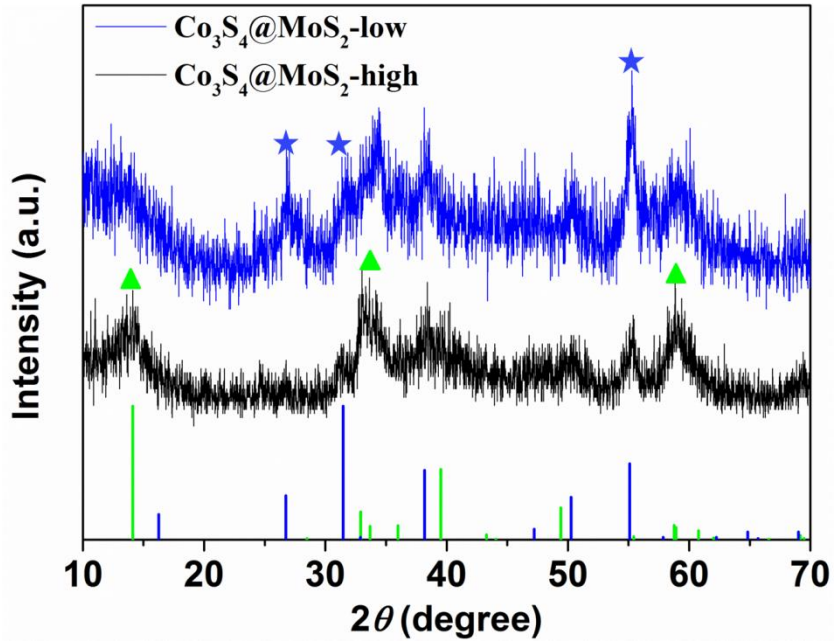

Figure S6. XRD patterns of synthesized Co_3S_4@MoS_2-low and Co_3S_4@MoS_2-high. Blue vertical lines indicate the reference pattern of Co_3S_4 (JCPDS card no. 47-1738), and green vertical lines indicate the reference pattern of MoS_2 (JCPDS card no. 75-1539).

Note for Figure S6: As shown in **Figure S6**, Co_3S_4@MoS_2-low and Co_3S_4@MoS_2-high both exhibit XRD patterns similar to those of hollow Co_3S_4@MoS_2 heterostructures (**Figure 3a**), which proves the existence of hexagonal MoS_2 and cubic Co_3S_4. Co_3S_4@MoS_2-high shows stronger intensity at diffraction peaks of 14.1°, 32.9°, and 58.8° (indicated by green triangles in **Figure S6**) that are indexed, respectively, to the (002), (100), and (110) planes of hexagonal MoS_2, as compared with Co_3S_4@MoS_2-low. In contrast, Co_3S_4@MoS_2-low shows more obvious diffraction peaks located at 26.7°, 31.5°, and 55.1° (indicated by blue stars in **Figure S6**) that belong, respectively, to the (220), (311), and (440) planes of cubic Co_3S_4 phase, as compared with Co_3S_4@MoS_2-high. These results imply that the relative ratio of MoS_2 to Co_3S_4 increases from the Co_3S_4@MoS_2-low sample to the Co_3S_4@MoS_2-high sample.

Figure S7

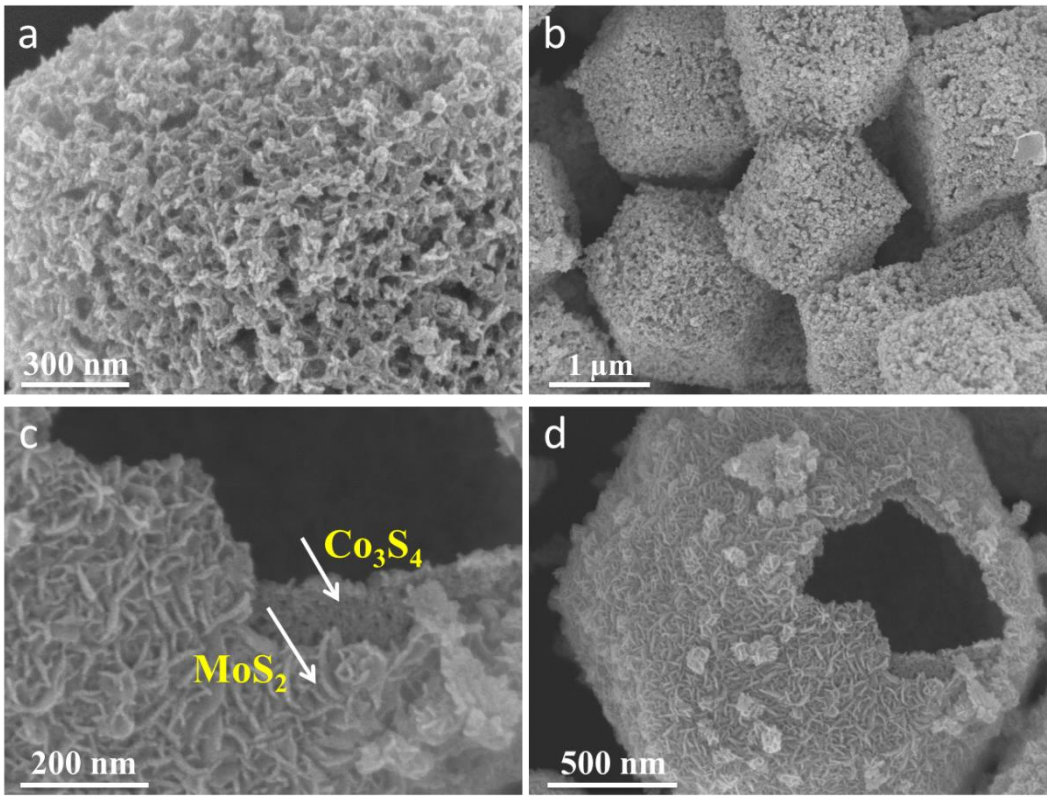

Figure S7. SEM images of (a,b) Co_3S_4@MoS_2-low and (c,d) Co_3S_4@MoS_2-high.

Note for Figure S7: It is clear that Co_3S_4@MoS_2-high (**Figure S7c**) consists of many more MoS_2 nanosheets as compared with Co_3S_4@MoS_2-low (**Figure S7a**).

Figure S8

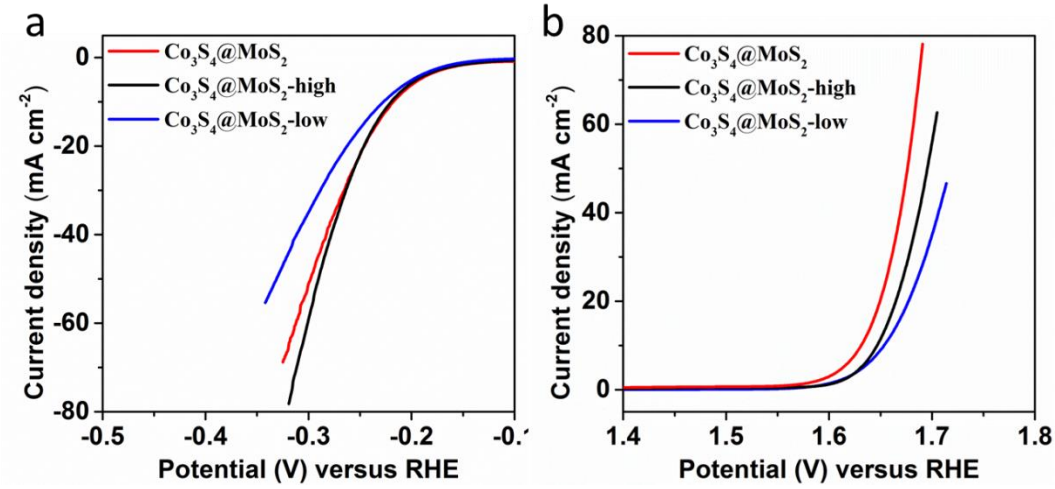

Figure S8. Polarization curves of Co_3S_4@MoS_2-low, Co_3S_4@MoS_2, and Co_3S_4@MoS_2-high electrodes in (a) 0.5 M H_2SO_4 and (b) 1 M KOH. All results shown are corrected by iR compensation. LSV scan rate: 5 mV·s^{-1}.

Note for Figure S8: The electrochemical activities of Co_3S_4@MoS_2 would be influenced by the thickness of MoS_2 nanosheets. As described in **Figure S8**, Co_3S_4@MoS_2-low displays the worst performances for both HER and OER. When the ratio of MoS_2 to Co_3S_4 is increased to a mediate ratio, Co_3S_4@MoS_2 exhibits increased catalytic activities for both HER and OER, as compared with Co_3S_4@MoS_2-low. However, the excessive MoS_2 do not favor the catalysis of HER and OER. The Co_3S_4@MoS_2-high sample possesses a similar catalytic activity for HER but worse catalytic activity for OER, as compared with Co_3S_4@MoS_2. The results demonstrate that the electrocatalytic performance of Co_3S_4@MoS_2 heterostructures for HER and OER can be adjusted and optimized by tuning the thickness of MoS_2 nanosheets.

According to the previous reports and discussion, MoS_2 and Co_3S_4 are active for catalyzing HER and OER, respectively. The worst HER and OER performance of Co_3S_4@MoS_2-low may be ascribed to its thin MoS_2 nanosheets or less active sites on the interfaces of Co_3S_4 and MoS_2. When excessive MoS_2 is coated on the surface of Co_3S_4, the inferior OER activity of Co_3S_4@MoS_2-high may be due to the fact that thicker MoS_2 nanosheets impede the activity of the inner Co_3S_4 layer. This result proves that the electrocatalytic performance of Co_3S_4@MoS_2 heterostructures for HER and OER can be modulated by tuning the thickness of MoS_2 nanosheets.

Figure S9

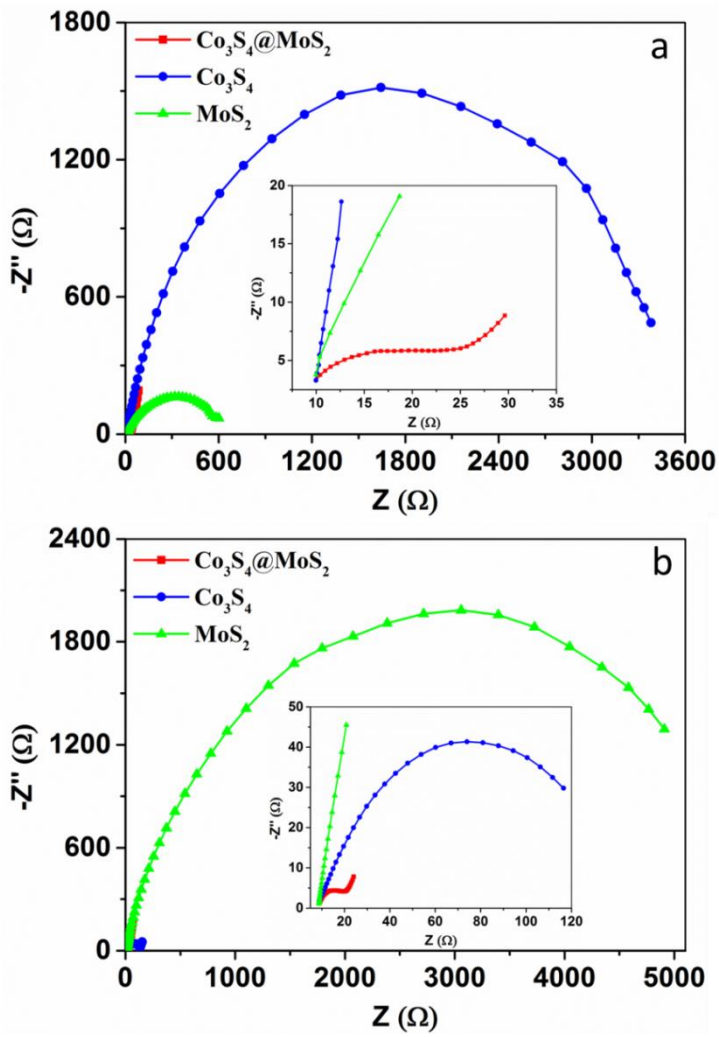

Figure S9. Nyquist plots of Co_3S_4@MoS_2, MoS_2, and Co_3S_4 collected at (a) -0.15 V *vs.* RHE in 0.5 M H_2SO_4 and (b) at 1.5 V *vs.* RHE in 1 M KOH.

Note for Figure S9: As shown in **Figure S9**, the Nyquist plot of Co_3S_4@MoS_2 has a much smaller semicircle in the high frequency region than do Co_3S_4 and MoS_2, indicating the lower intrinsic ohmic resistance of the Co_3S_4@MoS_2 electrode and electrolyte. This mainly contributes to the increased electrical conductivity of Co_3S_4@MoS_2 heterostructures, as compared with pure Co_3S_4 and MoS_2. The possible electronic interaction between cobalt sulfide and molybdenum disulfide has been investigated by other researchers. Ramos *et al.*[S1] proposed a model for Co_9S_8/MoS_2 interface based on density functional theory analysis and showed the creation of open latent vacancy sites on Mo atoms interacting with cobalt and the formation of Co-Mo bonds. The strong electron donation from Co to Mo also occurred through the intermediate sulfur atom's bonding to both metals; thus, an enhanced metallic character is observed. The intrinsic electrical conductivity of the Co_9S_8/MoS_2 heterostructure is, therefore, increased. Furthermore, some reports[S2,S3] have proved that the doping of transition metal atoms (*e.g.*, Co, Ni) could modulate and optimize the electronic structure of molybdenum disulfide and lead to increased electrical conductivity.

Figure S10

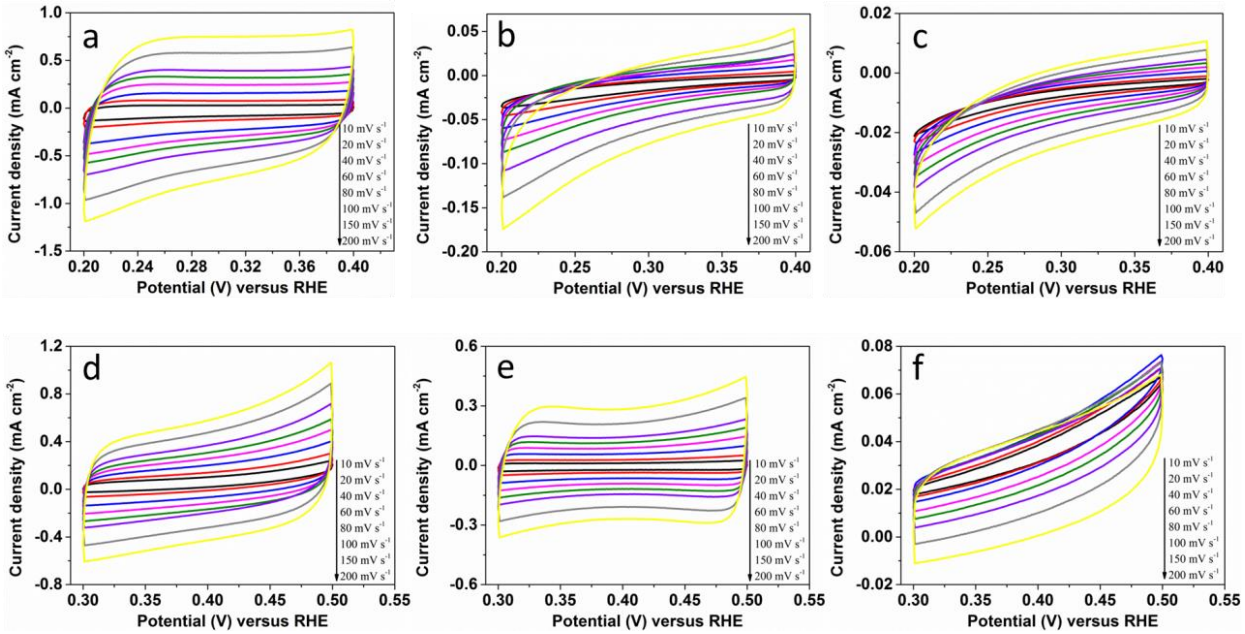

Figure S10. Cyclic voltammograms of (a) Co_3S_4@MoS_2, (b) MoS_2, (c) Co_3S_4 with various scan rates in 0.5 M H_2SO_4, and (d) Co_3S_4@MoS_2, (e) Co_3S_4, and (f) MoS_2 with various scan rates in 1 M KOH.

Figure S11

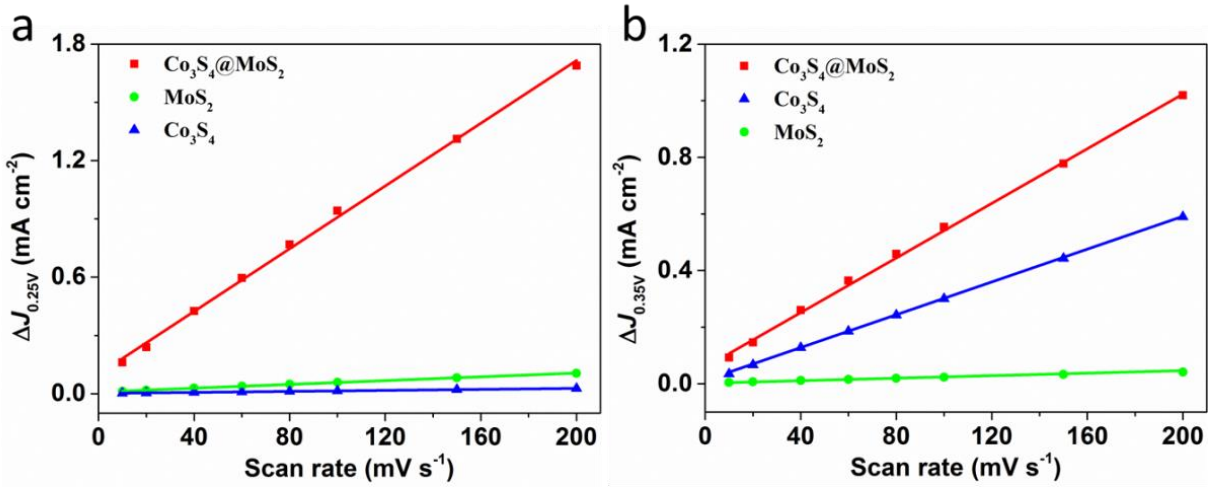

Figure S11. Linear slopes were plotted from the cyclic voltammograms (**Figure S10**) of Co_3S_4@MoS_2, MoS_2, and Co_3S_4 in (a) 0.5 M H_2SO_4 and (b) 1 M KOH. The linear slopes are equivalent to twice the double-layer capacitance (C_{dl}).

Figure S12

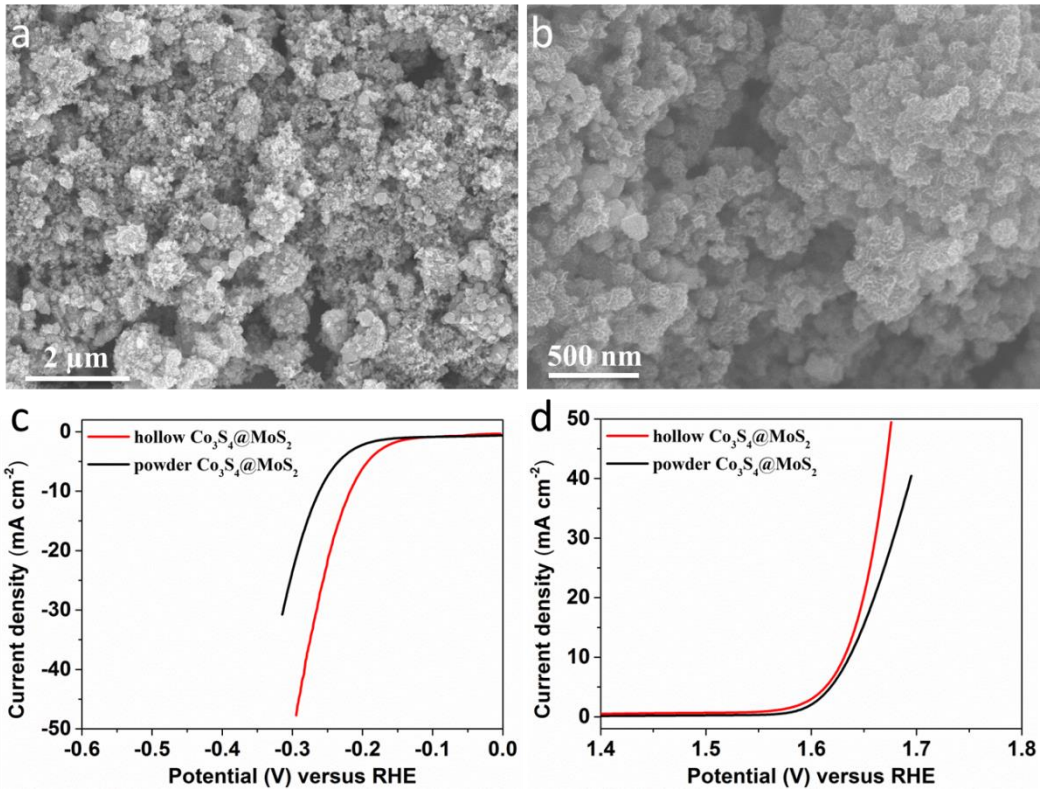

Figure S12. (a, b) SEM images of powder Co_3S_4@MoS_2 after long-term grinding and ultrasonication, and polarization curves of powder Co_3S_4@MoS_2 in (c) 0.5 M H_2SO_4 and (d) 1 M KOH. All results shown are corrected by iR compensation. LSV scan rate: 5 mV·s^{-1}.

Figure S13

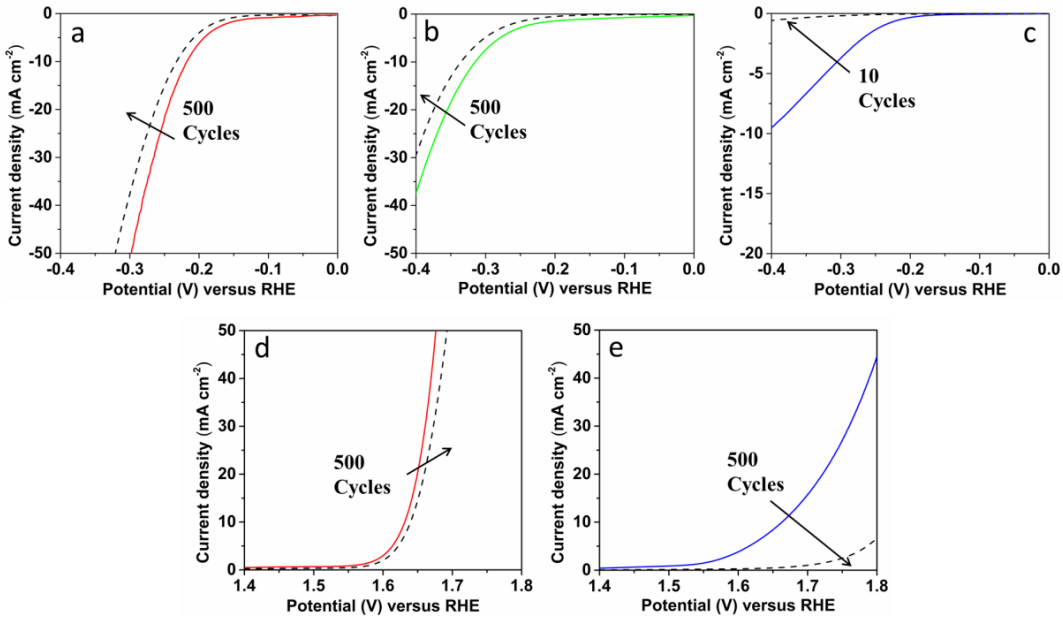

Figure S13. LSV curves of (a) Co_3S_4@MoS_2 and (b) MoS_2 obtained from the first and the 500th cycles, (c) Co_3S_4 obtained from the first and tenth cycles in 0.5 M H_2SO_4; LSV curves of (d) Co_3S_4@MoS_2 and (e) Co_3S_4 from the first and 500th cycles in 1 M KOH.

Figure S14

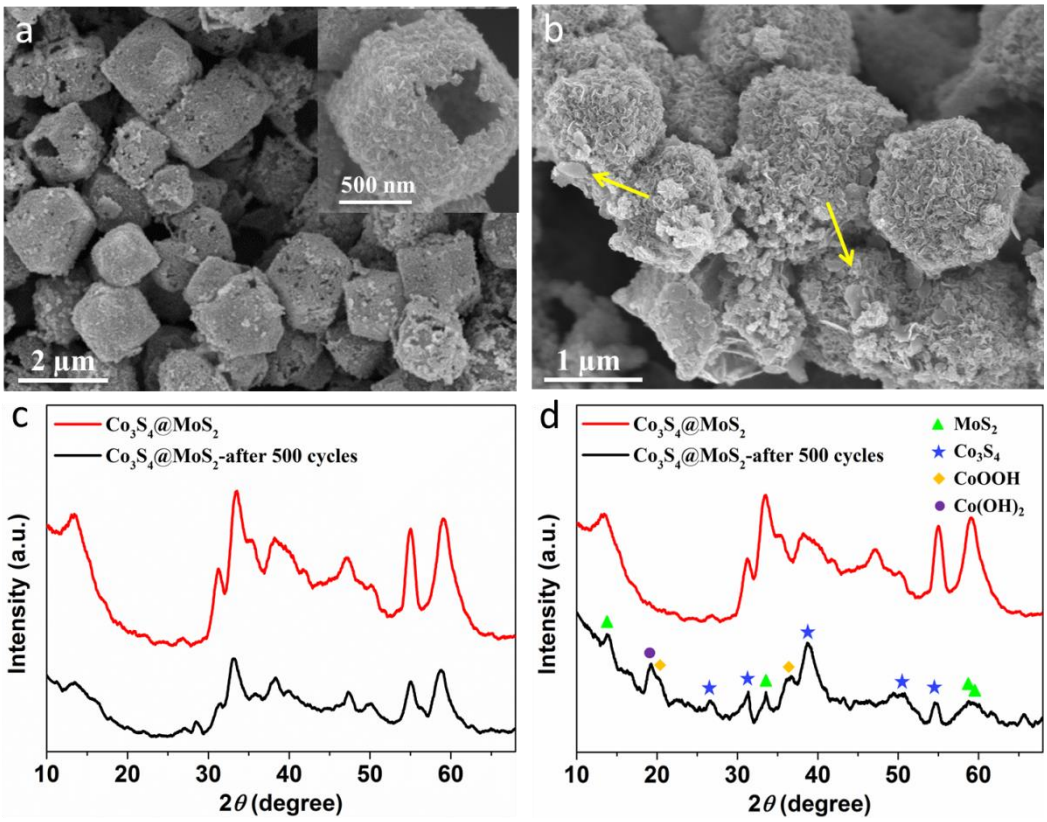

Figure S14. SEM images and XRD patterns of Co_3S_4@MoS_2 after 500 cycles of continuous CV measurements in (a,c) 0.5 M H_2SO_4, and (b,d) 1 M KOH.

Note for Figure S14: As observed in **Figure S14a–b**, although some cracked particles can be observed, Co_3S_4@MoS_2 almost maintains its original morphology after stability tests for both HER and OER, demonstrating its structural stability in both acid and alkaline electrolytes. However, after the OER process, some nanoplates are also observed on the polyhedrons. XRD measurement was also carried out to further determine the composition of the catalysts after stability tests in both acid and alkaline environments. **Figure S14c** shows that Co_3S_4@MoS_2 keeps the identical phase structure after 500 cycles of continuous CV measurements in 0.5 M H_2SO_4. As seen in **Figure S14d**, Co_3S_4 and MoS_2 phases are still visible, and they are the main components in the composite after the OER stability test. Some new peaks indexed to the $Co(OH)_2$ (JCPDS card no. 30-0443) and CoOOH (JCPDS card no. 07-0619) phases are also observed, which probably can be attributed to the new nanoplates on the Co_3S_4@MoS_2 polyhedrons (**Figure S14b, d**).

Figure S15

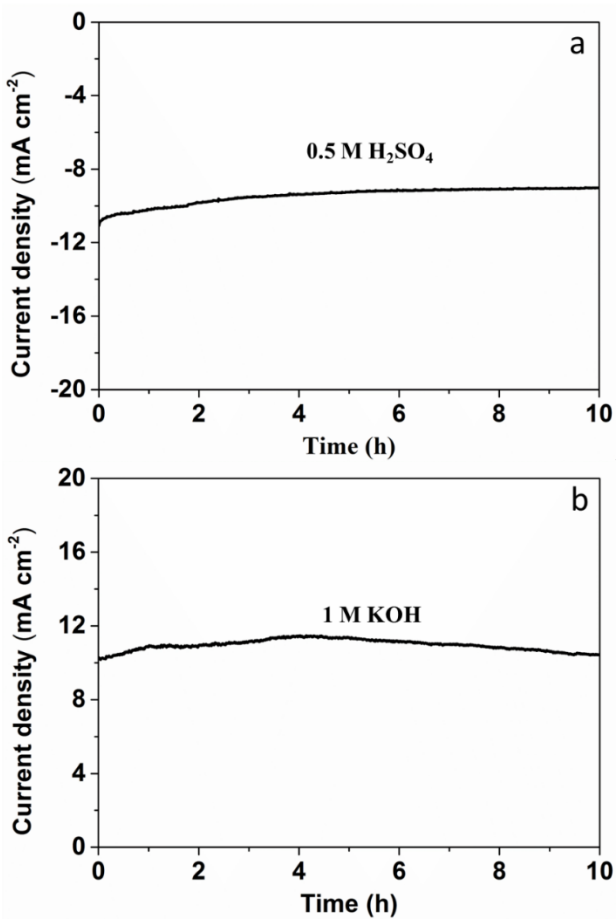

Figure S15. Chronoamperometric responses (*i–t*) recorded on the Co_3S_4@MoS_2 electrode (a) at a constant applied potential of -0.21 V *vs.* RHE over 10 h in 0.5 M H_2SO_4 and (b) at a constant applied potential of 1.59 V *vs.* RHE in 1 M KOH

Table S1. Comparison of HER performance of Co_3S_4@MoS_2 with other electrocatalysts

Catalysts	Current density (j, mA cm^{-2})	η at corresponding j (mV)	Tafel slope (mV·dec^{-1})	Electrolytes
Co_3S_4@MoS_2 (this work)	10	210	88	0.5 M H_2SO_4
MoO_3-MoS_2[S4]	10	~310	50-60	0.5 M H_2SO_4
MoS_2 microboxes[S5]	10	475	134	0.5 M H_2SO_4
MoN/C[S6]	2	290	54.5	0.1 M $HClO_4$
Nanoporous Mo_2C nanowire[S7]	60	200	53	0.5 M H_2SO_4
Double-gyroid MoS_2/FTO[S8]	2	190	50	0.5 M H_2SO_4
Defect-rich MoS_2[S9]	13	200	50	0.5 M H_2SO_4
$MoS_{2.7}$@NPG[S10]	10	210	41	0.5 M H_2SO_4
Co_9S_8@MoS_2/CNFs[S11]	10	190	110	0.5 M H_2SO_4
$CoMoS_3$ hollow prism[S12]	10	171	56.9	0.5 M H_2SO_4
Co-NRCNTs[S13]	10	260	69	0.5 M H_2SO_4
FeCo@NCNTs–NH[S14]	10	320	72	0.1 M H_2SO_4
CoNi@NC[S15]	10	140	104	0.1 M H_2SO_4

Table S2. Comparison of OER performance for Co_3S_4@MoS_2 with other electrocatalysts

Catalysts	Current density (j, mA cm^{-2})	η at corresponding j (mV)	Tafel slope (mV·dec^{-1})	Electrolytes
Co_3S_4@MoS_2 (this work)	10	310	59	1 M KOH
CoO@N/S-CNF[S16]	10	251	95	0.1 M KOH
Co_3O_4/$NiCo_2O_4$[S17]	10	340	88	1 M KOH
NiCo-NS[S18]	10	334	41	1 M KOH
Co-P Film[S19]	10	345	47	1 M KOH
Co_9S_8@MoS_2/CNFs[S11]	10	361	61	1 M KOH
MoS_2/Ni_3S_2[S20]	10	218	88	1 M KOH
Ni_3S_2/Ni foam[S21]	10	187	159	0.1 M KOH
n-NiFe LDH/NGF[S22]	10	337	45	0.1 M KOH
Co_3O_4/grapheme[S23]	10	~310	67	0.1 M KOH
Carbon Paper/Carbon Tubes/Cobalt-Sulfide[S24]	10	306	72	1 M KOH
Nanoporous hollow Co_3S_4 Nanosheets[S25]	10	363	90	0.1 M KOH
NiCo LDHs[S26]	10	367	40	1 M KOH
PNG-$NiCo_2O_4$[S27]	10	~349	156	0.1 M KOH
Co-P/NC[S28]	10	354	52	1 M KOH
Co-CNT/PC[S29]	10	315	74	0.1 M KOH
Co_3ZnC/Co@CN[S30]	10	366	81	1 M KOH
$CoSe_2$[S31]	10	430	50	1 M KOH
NNCNTAs[S32]	10	460	65	0.1 M KOH
Zn-Co-LDH nanosheets[S33]	10	~480	101	0.1 M KOH

Supporting References

[S1] M. Ramos, G. Berhault, D. A. Ferrer, B. Torres, R. R. Chianelli, HRTEM and Molecular Modeling of the MoS_2–Co_9S_8 Interface: Understanding the Promotion Effect in Bulk HDS Catalysts. *Catal. Sci. Technol*. **2012**, *2*, 164-178.

[S2] Yu, X. Y.; Feng, Y.; Jeon, Y.; Guan, B.; Lou, X. W.; Paik, U. Formation of Ni–Co–MoS_2 Nanoboxes with Enhanced Electrocatalytic Activity for Hydrogen Evolution. *Adv. Mater.* **2016**, *28*, 9006-9011.

[S3] Wang, H. T.; Tsai, C.; Kong, D. S.; Chan, K. R.; Pedersen, F. A.; Nørskov, J. K.; Cui, Y. Transition-metal Doped Edge Sites in Vertically Aligned MoS_2 Catalysts for Enhanced Hydrogen Evolution. *Nano Res.* **2015**, *8*, 566-575.

[S4] Chen, Z. B.; Cummins, D.; Reinecke, B. N.; Clark, E.; Sunkara, M. K.; Jaramillo, T. F. Core–shell MoO_3–MoS_2 Nanowires for Hydrogen Evolution: A Functional Design for Electrocatalytic Materials. *Nano lett*. **2011**, *11*, 4168-4175.

[S5] Zhang, L.; Wu, H. B.; Yan, Y.; Wang, X.; Lou, X. W. Hierarchical MoS_2 Microboxes Constructed by Nanosheets with Enhanced Electrochemical Properties for Lithium Storage and Water Splitting. *Energy Environ. Sci*. **2014**, *7*, 3302-3306.

[S6] Chen, W. F.; Sasaki, K.; Ma, C.; Frenkel, A. I.; Marinkovic, N.; Muckerman, J. T.; Zhu, Y. M.; Adzic, R. R. Hydrogen-Evolution Catalysts Based on Non-Noble Metal Nickel–Molybdenum Nitride Nanosheets. *Angew. Chem. Int. Ed.* **2012**, *51*, 6131-6135.

[S7] Liao, L.; Wang, S. N.; Xiao, J. J.; Bian, X. J.; Zhang, Y. H.; Scanlon, M. D.; Hu, X. L.; Tang, Y.; Liu, B. H.; Girault, H. H. A Nanoporous Molybdenum Carbide Nanowire as an Electrocatalyst for Hydrogen Evolution Reaction. *Energy Environ. Sci*. **2014**, *7*, 387-392.

[S8] Kibsgaard, J.; Chen, Z. B.; Reinecke, B. N.; Jaramillo, T. F. Engineering the Surface

Structure of MoS_2 to Preferentially Expose Active Edge Sites for Electrocatalysis. *Nat. Mater.* **2012**, *11*, 963-969

[S9] Xie, J. F.; Zhang, H.; Li, S.; Wang, R. X.; Sun, X.; Zhou, M.; Zhou, J. F.; Lou, X. W.; Xie, Y. Defect-Rich MoS_2 Ultrathin Nanosheets with Additional Active Edge Sites for Enhanced Electrocatalytic Hydrogen Evolution. *Adv. Mater*. **2013**, *25*, 5807-5813.

[S10] Ge, X. B.; Chen, L. Y.; Zhang, L.; Wen, Y. R.; Hirata, A.; Chen, M. W. Nanoporous Metal Enhanced Catalytic Activities of Amorphous Molybdenum Sulfide for High-Efficiency Hydrogen Production. *Adv. Mater*. **2014**, *26*, 3100-3104.

[S11] Zhu, H.; Zhang, J.F.; Yanzhang, R. P.; Du, M. L.; Wang, Q. F.; Gao, G. H.; Wu, J. D.; Wu, G. M.; Zhang, M.; Liu, B.; Yao, J. M.; Zhang, X. W. When Cubic Cobalt Sulfide Meets Layered Molybdenum Disulfide: a Core–shell System toward Synergetic Electrocatalytic Water Splitting. *Adv. Mater*. **2015**, *27*, 4752-4759.

[S12] Le, L.; Xia, B. Y.; Wang, X.; Lou, X. W. General Formation of M–MoS_3 (M = Co, Ni) Hollow Structures with Enhanced Electrocatalytic Activity for Hydrogen Evolution. *Adv. Mater*. **2016**, *28*, 92-97.

[S13] Zou, X. X.; Huang, X. X.; Goswami, A.; Silva, R.; Sathe, B. R.; Mikmekova, E.; Asefa, T. Cobalt-Embedded Nitrogen-Rich Carbon Nanotubes Efficiently Catalyze Hydrogen Evolution Reaction at All pH Values. *Angew. Chem. Int. Ed.* **2014**, *53*, 4372-4376.

[S14] Deng, J.; Ren, P. J.; Deng, D. H.; Yu, L.; Yang, F.; Bao, X. H. Highly Active and Durable Non-precious-metal Catalysts Encapsulated in Carbon Nanotubes for Hydrogen Evolution Reaction. *Energy Environ. Sci*. **2014**, *7*, 1919-1923.

[S15] Deng, J.; Ren, P. J.; Deng, D. H.; Bao, X. H. Enhanced Electron Penetration through an Ultrathin Graphene Layer for Highly Efficient Catalysis of the Hydrogen Evolution Reaction.

Angew. Chem. Int. Ed. **2015**, *54*, 2100-2104.

[S16] Liu, T.; Guo, Y. F.; Yan, Y. M.; Wang, F.; Deng, C.; Rooney, D.; Sun, K. N. CoO Nanoparticles Embedded in Three-dimensional Nitrogen/sulfur Co-doped Carbon Nanofiber Networks as a Bifunctional Catalyst for Oxygen Reduction/Evolution Reactions. *Carbon* **2016**, *106*, 84-92.

[S17] Hu, H.; Guan, B. Y.; Xia, B. Y.; Lou, X. W. Designed Formation of $Co_3O_4/NiCo_2O_4$ Double-Shelled Nanocages with Enhanced Pseudocapacitive and Electrocatalytic Properties. *J. Am. Chem. Soc.* **2015**, *137*, 5590-5595.

[S18] Song, F.; Hu, X. L. Exfoliation of Layered Double Hydroxides for Enhanced Oxygen Evolution Catalysis. *Nat. Commun.* **2014**, *5*, 4477.

[S19] Jiang, N.; You, B.; Sheng, M. L. Electrodeposited Cobalt-Phosphorous-Derived Films as Competent Bifunctional Catalysts for Overall Water Splitting. *Angew. Chem. Int. Ed.* **2015**, *54*, 6251-6254.

[S20] Zhang, J.; Wang, T.; Pohl, D.; Rellinghaus, B.; Dong, R. H.; Liu, S. H.; Zhuang, X. D.; Feng, X. L. Interface Engineering of MoS_2/Ni_3S_2 Heterostructures for Highly Enhanced Electrochemical Overall-water-splitting Activity. *Angew. Chem. Int. Ed.* **2016**, *55*, 6702-6707.

[S21] Zhou, W. J.; Wu, X. J.; Cao, X. H.; Huang, X.; Tan, C. L.; Tian, J.; Liu, H.; Wang, J. Y.; Zhang, H. Ni_3S_2 Nanorods/Ni Foam Composite Electrode with Low Overpotential for Electrocatalytic Oxygen Evolution. *Energy Environ. Sci*. **2013**, *6*, 2921-2924.

[S22] Tang, C.; Wang, H. S.; Wang, H. F.; Zhang, Q.; Tian, G. L.; Nie, J. Q.; Wei, F. Spatially Confined Hybridization of Nanometer-Sized NiFe Hydroxides into Nitrogen-Doped Graphene Frameworks Leading to Superior Oxygen Evolution Reactivity. *Adv. Mater*. **2015**,

27, 4516-4522.

[S23] Ma, T. Y.; Dai, S.; Jaroniec, M.; Qiao, S. Z. Metal–Organic Framework Derived Hybrid Co_3O_4-Carbon Porous Nanowire Arrays as Reversible Oxygen Evolution Electrodes. *J. Am. Chem. Soc.* **2014**, *136*, 13925-13931.

[S24] Wang, J.; Zhong, H. X.; Wang, Z. L.; Meng, F. L.; Zhang, X. B. Integrated Three-Dimensional Carbon Paper/Carbon Tubes/Cobalt-sulfide Sheets as an Efficient Electrode for Overall Water Splitting. *ACS Nano* **2016**, *10*, 2342-2348.

[S25] Zhao, W. W.; Zhang, C.; Geng, F. Y.; Zhuo, S. F.; Zhang, B. Nanoporous Hollow Transition Metal Chalcogenide Nanosheets Synthesized via the Anion-Exchange Reaction of Metal Hydroxides with Chalcogenide Ions. *ACS Nano* **2014**, *8*, 10909-10919.

[S26] Liang, H. F.; Meng, F.; Cabán-Acevedo, M.; Li, L. S.; Forticaux, A.; Xiu, L. C.; Wang, Z. C.; Jin, S. Hydrothermal Continuous Flow Synthesis and Exfoliation of NiCo Layered Double Hydroxide Nanosheets for Enhanced Oxygen Evolution Catalysis. *Nano Lett.* **2015**, *15*, 1421-1427.

[S27] Chen, S.; Qiao, S. Z. Hierarchically Porous Nitrogen-Doped Graphene–NiCo2O4 Hybrid Paper as an Advanced Electrocatalytic Water-Splitting Material. *ACS Nano* **2013**, *7*, 10190-10196.

[S28] You, B.; Jiang, N.; Sheng, M. L.; Gul, S.; Yano, J. K.; Sun, Y. J. High-Performance Overall Water Splitting Electrocatalysts Derived from Cobalt-Based Metal–Organic Frameworks. *Chem. Mater*. **2015**, *27*, 7636-7642

[S29] Dou, S.; Li, X. Y.; Tao, L.; Huo, J.; Wang, S. Y. Cobalt Nanoparticle-embedded Carbon Nanotube/porous Carbon Hybrid Derived from MOF-encapsulated Co_3O_4 for Oxygen Electrocatalysis. *Chem. Commun*. **2016**, *52*, 9727-9730.

[S30] Su, J. W.; Xia, G. L.; Li, R.; Yang, Y.; Chen, J. T.; Shi, R. H.; Jiang, P.; Chen, Q. W. Co_3ZnC/Co Nano Heterojunctions Encapsulated in N-doped Graphene Layers Derived From PBAs as Highly Efficient Bi-functional OER and ORR Electrocatalysts. *J. Mater. Chem. A* **2016**, *4*, 9204-9212.

[S31] Kwak, I. H.; Im, H. S.; Jang, D. M.; Kim, Y. W.; Park, K. D.; Lim, Y. R.; Cha, E. H.; Park, J. $CoSe_2$ and $NiSe_2$ Nanocrystals as Superior Bifunctional Catalysts for Electrochemical and Photoelectrochemical Water Splitting. *ACS appl. Mater. Interfaces* **2016**, *8*, 5327-5334.

[S32] Zhao, Z. L.; Wu, H. X.; He, H. L.; Xu, X. L.; Jin, Y. D. A High-Performance Binary Ni–Co Hydroxide-based Water Oxidation Electrode with Three-Dimensional Coaxial Nanotube Array Structure. *Adv. Funct. Mater*. **2014**, *24*, 4698-4705.

[S33] Qiao, C.; Zhang, Y.; Zhu, Y. Q.; Cao, C. B.; Bao, X. H.; Xu, J. Q. One-step Synthesis of Zinc–cobalt Layered Double Hydroxide (Zn–Co-LDH) Nanosheets for High-efficiency Oxygen Evolution Reaction. *J. Mater. Chem. A* **2015**, *3*, 6878-6883.